Polymer 50 (2009) 1236–1245

Contents lists available at ScienceDirect

Polymer

journal homepage: www.elsevier.com/locate/polymer

Synthesis, characterization and self-assembly behavior in water as fluorescent sensors of cationic water-soluble conjugated polyfluorene-*b*-poly (*N*-isopropylacrylamide) diblock copolymers

Weizhi Wang*, Rui Wang, Chao Zhang, Su Lu, Tianxi Liu*

Key Laboratory of Molecular Engineering of Polymers of Ministry of Education, Department of Macromolecular Science, Laboratory of Advanced Materials, Fudan University, 220 Handan Road, Shanghai 200433, People's Republic of China

ARTICLE INFO

Article history:
Received 28 October 2008
Received in revised form
12 December 2008
Accepted 13 December 2008
Available online 24 December 2008

Keywords:
Water-soluble conjugated polymers
Self-assembly
Fluorescent sensors

ABSTRACT

A series of well-defined novel water-soluble diblock copolymers containing conjugated amino-terminal polyfluorene (PF) block and coil-like poly(*N*-isopropylacrylamide) (PNIPAM) have been successfully synthesized through atom transfer radical polymerization (ATRP) initiated by a 2-bromoisobutyrate end-capped PF macroinitiator using CuCl/HMTETA (1,1,4,7,10,10-hexamethyltriethylenetetramine) as the catalyst. The first-order kinetic plots indicate the presence of a constant number of active species during the polymerization. The molecular weight and molecular weight distribution can be well controlled, implying synthesis of well-defined block structures of the copolymers. The chemical structures of block copolymers have been characterized by ^{1}H NMR, UV–vis, and photoluminescence (PL) spectra. PF aggregates are formed in water with the increase of temperature for the conjugated-ionic diblock copolymer synthesized, as confirmed by dynamic light scattering (DLS). The formation of excimers within the PF aggregates results in improved Förster resonance energy transfer (FRET) efficiencies.

1. Introduction

Water-soluble conjugated polymers (WSCPs) have received considerable attention as sensing materials because of their high sensitivities to analytes. Their high sensitivities over devices using small molecules arise from collective optical and conducting properties of the conjugated polymers, which are extremely sensitive to minor external structural perturbations or to electron density changes within the polymer backbone in the presence of analytes [1–10]. A variety of WSCPs containing molecular recognition sites have been reported as sensing materials for DNA, RNA, and metal ions, such as poly(thiophene), poly(*p*-phenylene), poly(*p*-phenylene vinylene), polyfluorene, and poly(phenylene ethynylene) backbones [9–12]. The water-soluble properties are endowed by grafting quaternized ammonium, carboxylate, sulphonate or ethylene oxide side chains to a conjugated polymer. Furthermore, the structure can be linear, star, and dendrimer structure. All the WSCPs display an analogous ability to collect excitations and deliver them to focal points by energy-transfer mechanisms. However, the uncertainties in linear structure WSCPs (e.g. molecular weight and its distribution, structural defects) limit the determination of detailed relationships between molecular structures and optical properties. Therefore, WSCP dendrimer with precise structure was reported by Bazan and his coworkers and has been proved that such an attractive structure can adapt to the range of secondary structures presented by biological macromolecules [13–15]. However, the complex multi-step synthesis and high molecular weights (usually for reducing the solubility of conjugated polymers in water) make it a laborious work when preparing these materials.

Moreover, the sensitivity of WSCPs to analytes was controlled by the interface interaction between both of them [10]. WSCPs often exhibit large persistent lengths in solution and thus it can be considered as a one-dimensional conduit. The analyte therefore undergoes a one-dimensional random walk when the polymers are in solution, which is inefficient for quenching: the analyte visits the same receptor. If the analyte can be made to touch other WSCPs in different directions, much higher quenching factors can be achieved. Multi-dimension touch is easily achieved by aggregation of polymer (as shown in Scheme 1). However, greatly enhanced aggregation of WSCPs also will reduce the solubility of conjugated polymers in water.

In this contribution, a series of novel well-defined water-soluble diblock copolymers containing conjugated amino-terminal polyfluorene (PF) block and coil-like poly(*N*-isopropylacrylamide) (PNIPMA) were successfully synthesized through atom transfer radical polymerization (ATRP) initiated by a 2-bromoisobutyrate

* Corresponding authors. Tel.: +86 21 55664197; fax: +86 21 65640293.
E-mail addresses: weizhiwang@fudan.edu.cn (W.z. Wang), txliu@fudan.edu.cn (T.x. Liu).

0032-3861/$ – see front matter © 2008 Elsevier Ltd. All rights reserved.
doi:10.1016/j.polymer.2008.12.026

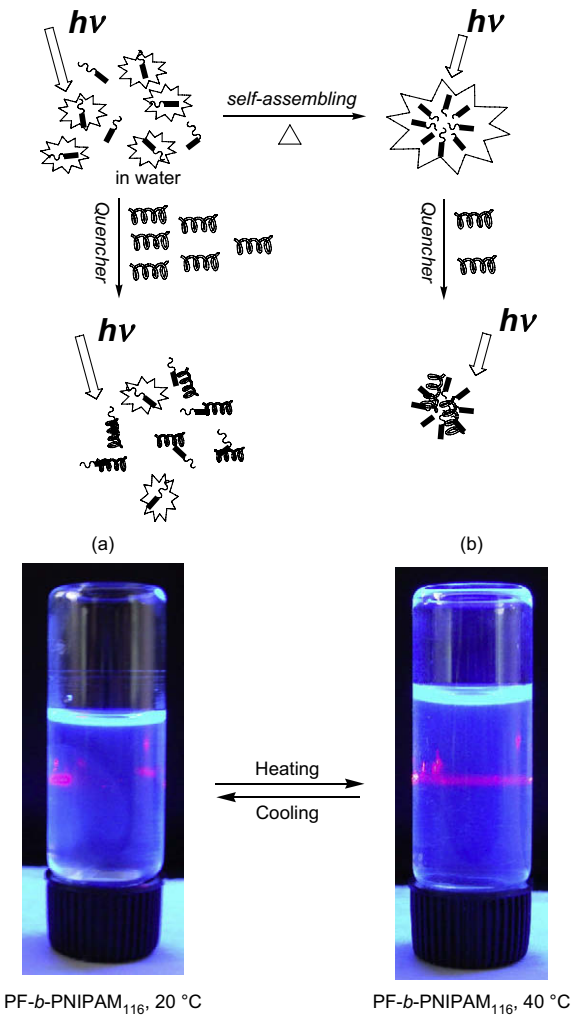

Scheme 1. Schematic illustration of the fabrication of micelles from PF-*b*-PNIPAM$_{116}$ diblock copolymer and their fluorescent quenching by traces of analytes. The digital photographs are temperature-dependent optical transmittance obtained for 1.0×10^{-5} M aqueous solution of fluorene chain: (a) PF-*b*-PNIPAM$_{116}$, 20 °C; (b) PF-*b*-PNIPAM$_{116}$, 40 °C.

end-capped PF macroinitiator using CuCl/HMTETA (1,1,4,7,10,10-hexamethyltriethylenetetramine) as the catalyst base on our previous work [16–18]. The water-soluble cationic rigid rod PF chains provide electrostatic interactions with the negatively charged analytes, such as DNA (or RNA). The coil "smart" chains of PNIPAM can assemble to a similar dendrimer structure with the change of temperature [19–26], which solves the conflict of solubility and the sensitivities of WSCPs to analytes. Therefore, the novel rod–coil structure combined not only the merits of linear (i.e., excellent solubility) but also the bonus of precisely structured dendrimer WSCP (i.e., easy interaction with analytes). This type of self-assembly behavior of cationic water-soluble conjugated diblock copolymers makes them potential candidates in optoelectronic and sensory applications.

2. Experimental

2.1. Materials

2,7-Dibromofluorene (97%), *N*-isopropylacrylamide (NIPAM) (98%), benzene-1,4-diboronic acid, 3-dimethylaminopropylchloride hydrochloride (98%), 4-bromobenzyl alcohol (99%), phenylboronic acid, 1,1,4,7,10,10-hexamethyltriethylenetetramine (HMTETA) (97%), 2-bromoisobutyryl bromide (BiBB) (98%), CuCl (99.995%+), *N*,*N*-dimethylformamide (DMF, 99.9%, TEDIA), dichloromethane (99.9%, TEDIA), and bromoethane (99%, Merck) were distilled from calcium hydride (CaH_2) and stored under argon. Tetrahydrofuran (99.8%, TEDIA) and toluene (99.5%, Merck) were distilled from sodium/benzophenone. Other chemicals and reagents were purchased from Aldrich and Acros Chemical Co. unless otherwise stated and used without further purification. All of the solvents were used after purification according to conventional methods when required.

2.2. Measurements and characterization

^{1}H, ^{13}C NMR spectra were recorded with Varian Mercury Plus 400 spectrometers, and chemical shifts were reported in ppm units with tetramethylsilane as the internal standard. Infrared spectra were measured with KBr pellets on a Shimadzu IR Prestige-21 spectrometer, where the percentage of transmittance vs the wavenumber (in cm^{-1}) was plotted. A Shimadzu DTG-60H thermal analyzer was used to record thermogravimetric analysis (TGA) under a heating rate of 10 °C/min and a nitrogen flow rate of 20 mL/min. Elemental analyses were performed on a Vario EL Elemental Analysis Instrument (Elementar Co.). The UV–vis absorption spectra were obtained in chloroform on a Shimadzu UV-3150 spectrophotometer. The photoluminescence spectra were recorded on a Shimadzu RF-5301 PC fluorometer at room temperature.

The fluorescence quantum yields (Φ_f) of the polymers in solutions were recorded by using the diluted quinoline solution in 0.1 N H_2SO_4 as the standard, assuming that the fluorescence quantum yield was 0.546 with the excitation wavelength of 365 nm. Φ_f was calculated according to the following equation:

$$\Phi_S = \Phi_R \left(\frac{A_R}{A_S}\right)\left(\frac{I_S}{I_R}\right)\left(\frac{N_S^2}{N_R^2}\right) \quad (1)$$

where Φ_R and Φ_S are the fluorescence quantum yields of quinoline and the polymer, respectively. A_R and A_S are the absorbances of quinoline and the polymers at the excitation wavelength, respectively. I_R and I_S are the integrated emission intensities of quinoline and the polymers, respectively. N_R and Ns are refractive indices of the corresponding solvents of the solutions, respectively. In the cases where mixed solvents were employed, the refractive indices of the mixed solvents were calculated according to Eq. (2) as follows:

$$N_{mix}^2 = F_A N_A^2 + F_B N_B^2 \quad (2)$$

where F_A and F_B are the fractions (vol/vol) of solvents A and B, respectively.

Molecular weights and polydispersities of polymers were determined by gel permeation chromatography (GPC) analysis with polystyrene as the standard. Molecular weight measurements of water-soluble polymer samples were performed at room temperature in 0.1 M $NaNO_3$ aqueous solution using a Waters Ultrahydrogel column containing cross-linked methacrylate gel as the matrix material at a flow rate of 0.67 mL/min. Light scattering measurements were performed using a Wyatt Technology DAWN-F DSP instrument equipped with an He–Ne laser ($\lambda_o = 632.8$ nm), and duplicate measurements were performed in all cases. The weight-average molecular weight (M_w), number-average molecular weight (M_n), and the polydispersity index (M_w/M_n) were obtained using Astra software. Dynamic light scattering (DLS) experiments were performed using a Brookhaven Instruments 128-channel BI-2030 AT digital correlator equipped with a Spectraphysics He–Ne laser

operating at 632.8 nm. Measurements were made at 90°. The block copolymer samples were prepared as 0.15 g/L solutions in water. All samples were prepared by filtering about 1 mL of the aqueous solution with a 0.45 μm Millipore filter into a clean scintillation vial and heating at a given temperature for about 1 h and then characterized by DLS (Scheme 2).

2.3. 2,7-Dibromo-9,9-bis(3′-(N,N-dimethylamino)propyl)-fluorene (**1**) [27]

The synthesis route was reported in the literature [27]. ^{1}H NMR (400 MHz, DMSO-d_6): δ 7.82–7.80 (d, 2H, fluorene ring), 7.69 (s, 2H, fluorene ring), 7.56–7.53 (d, 2H, fluorene ring), 2.04–2.00 (t, 4H, –CH_2N), 1.92–1.88 (m, 16H, –NCH_3, –CH_2–), 0.60–0.52 (m, 4H, –CH_2–). ^{13}C NMR (100 MHz, $CDCl_3$): δ 152.37, 139.50, 130.75, 126.51, 122.04, 121.58 (C-fluorene ring), 60.01 (–CH_2N), 55.70 (C9-fluorene ring), 45.78 (–NCH_3), 37.96 (–CH_2–), 22.42 (–CH_2–). Elem. Anal. Calcd. for $C_{23}H_{30}Br_2N_2$: C, 55.89; H, 6.12; N, 5.67. Found: C, 55.76; H, 6.12; N, 5.60.

2.4. Synthesis of hydroxy-functionalized poly[(9,9-bis(3′-(N,N-dimethylamino)propyl)-2,7-fluorene)-alt-1,4-phenylene] (PF–OH)

Into a mixture of (**1**) (0.9 g, 1.8 mmol), benzene-1,4-diboronic acid (0.3 g, 1.8 mmol), $Pd(PPh_3)_4$ (25 mg), and K_2CO_3 (1.0 g, 7.3 mmol) in 30 mL of THF and 10 mL of water were degassed and stirred at 80 °C for 2 h, and then phenylboronic acid (31 mg, 0.26 mmol) and 4-bromobenzyl alcohol (49 mg, 0.26 mmol) in 60 mL of anhydrous toluene were added. The mixture was concentrated, and the desired polymer was precipitated from acetone (0.54 g, 72%) to give final product as yellow powder with M_n of 2500 (GPC) and 2400 (^{1}H NMR) and M_w/M_n of 1.6. ^{1}H NMR (400 MHz, $CDCl_3$): δ 7.92–7.67 (m, fluorene ring), 7.65–7.50 (m, benzene ring), 4.81 (–Ph–CH_2–OH), 2.18–2.05 (m, –NCH_2–), 2.05–1.98 (m, –NCH_3), 1.76, 0.99. ^{13}C NMR (100 MHz, $CDCl_3$): δ 152.36, 151.59, 140.78, 140.64, 140.18, 139.49, 130.80, 129.23, 128.59, 127.95, 127.45, 126.63, 126.57, 122.03, 121.74, 121.64, 120.63, 60.24, 55.40, 45.70, 38.34, 22.38.

2.5. Poly[(9,9-bis(3′-((N,N-dimethyl)-N-ethylammonium)-propyl)-2,7-fluorene)-alt-1,4-phenylene] bromide (PF–Br)

PF–OH (1.35 g, 0.54 mmol), triethylamine (4.4 mL, 31 mmol), and dry DMSO (40 mL) were placed in a 150 mL round-bottomed flask. After cooling to 0 °C, 2-bromoisobutyryl bromide (3.6 mL, 26 mmol) was added dropwise with vigorous stirring under an argon atmosphere. The temperature was allowed to rise to 20 °C, and the reaction mixture was stirred overnight. After filtration, methanol was added into the solution to remove the excess of bromoisobutyryl bromide, and bromo-ended PF macroinitiator was precipitated in acetone. The solid was rinsed with methanol

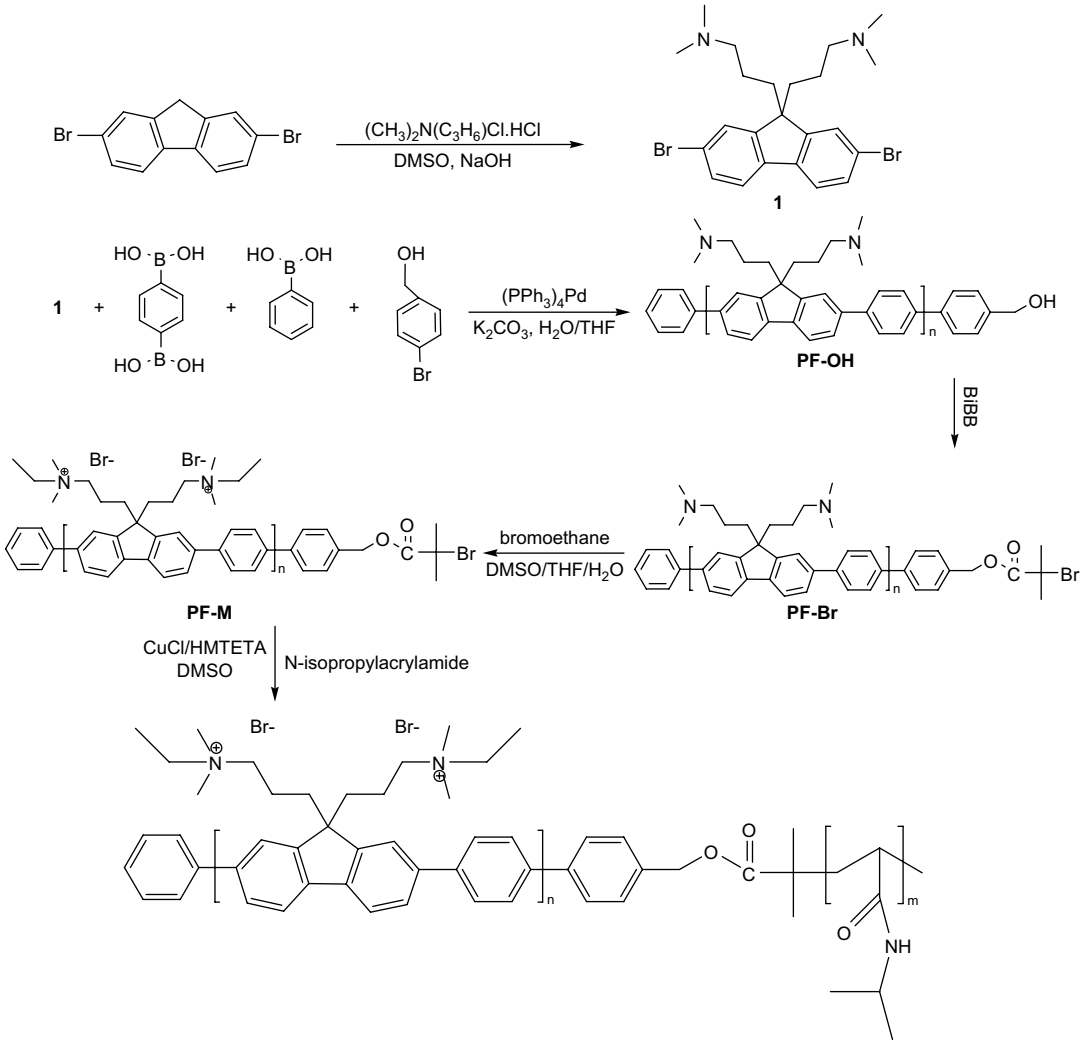

Scheme 2. Synthetic routes for diblock copolymers.

sufficiently and passed through a short column using DMF as the eluent. After it was dried under vacuum at 40 °C, 1.6 g of faint yellow product was obtained (85% in yield) with M_n of 2600 (GPC) and 2700 (^{1}H NMR) and M_w/M_n of 1.5. ^{1}H NMR (400 MHz, $CDCl_3$): δ 7.92–7.67 (m, fluorene ring), 7.65–7.50 (m, benzene ring), 5.31 (Ph–CH_2–OC═O), 2.13–2.02 (m, –NCH_2–, –NCH_3), 1.78, 1.32, 0.89. ^{13}C NMR (100 MHz, $CDCl_3$): δ 170.02, 149.41, 140.55, 139.22, 138.49, 135.67, 130.90, 129.56, 128.85, 127.55, 126.51, 125.50, 124.44, 121.67, 67.98, 59.94, 50.12, 42.11, 39.74, 20.15.

2.6. Synthesis of water-soluble PF macroinitiators (PF-M)

100 mg of PF–Br was treated with bromoethane in DMSO/THF (1:4). Once some precipitations were observed, some water was added to the solution to dissolve the precipitation. After the reaction was stirred at 25 °C for 5 days, ether was added and the mixture was extracted with water. The aqueous layer was concentrated and the residue was precipitated from THF and dried overnight in a vacuum at 30 °C to yield PF-M (69%). ^{1}H NMR (400 MHz, DMSO-d_6): δ 8.10–7.90 (br, ring aromatic protons), 7.63, 7.53 (phenyl end groups), 5.31 (s, Ph–CH_2O–), 3.40–3.20 (br, –NCH_2, –NCH_3), 1.80–1.92 (–$C(CH_3)_2$Br), 1.4–1.2 (m, –CH_2, –CH_3). ^{13}C NMR ($CDCl_3$, ppm): δ 171.61, 151.87 (fluorene), 141.84 (w), 140.55 (fluorene), 140.01 (fluorene), 139.44 (w), 134.21 (w, phenylene), 128.40 (phenylene), 127.38 (phenylene), 126.16 (fluorene), 121.53 (fluorene), 119.99 (fluorene), 67.46 (Ph–C–O), 55.33 (Ph–C–Ph), 40.38 (CH_2), 31.44 (CH_2), 30.87 (CH_3), 29.62 (CH_2), 23.88 (CH_2), 22.55 (CH_2), 14.04 (CH_3). FTIR (KBr, cm^{-1}): 3059, 3026, 2960, 2926, 2854 (–C–H); 1737, 1458, 1156, 1105 (–C–O–C); 813.

2.7. Synthesis of water-soluble PF–PNIPAM diblock copolymers by ATRP

PF–PNIPAM diblock copolymers were synthesized by solution polymerization in DMSO. In a typical run, a glass tube was charged with 0.05 g (0.018 mmol) of PF macroinitiator and 3.6 mg (0.036 mmol) of CuCl before it was sealed with a rubber septum. The tube was degassed with three vacuum–argon cycles to remove air and moisture, and then DMSO (0.80 mL) and HMTETA (0.036 mmol) were added with syringes. The glass reactor was immersed in an oil bath at 60 °C, and a clear solution with light green color formed within a few seconds. Upon dissolution, 4.8 mmol of NIPAM was quickly injected into the tube to carry out the polymerization. Samples for ^{1}H NMR and GPC characterization were taken out from the reaction mixture at time intervals. The samples were passed through a column of neutral alumina to remove the catalysts. The polymers were precipitated into excess of hexane and dried in a vacuum at 40 °C. Light yellow powdery to glassy samples were obtained.

3. Results and discussion

3.1. Synthesis of water-soluble PF macroinitiators

Hydroxy-functionalized polyfluorene macroinitiators have been synthesized previously through a one-pot reaction [17,18]. For this purpose, a PF polymer end-capped with hydroxyl groups was prepared by using Pd(0) catalyst through an intermolecular Suzuki-type condensation. 4-Bromobenzyl alcohol and phenylboronic acid as the end-capper in the flask after the condensation reaction at 80 °C for 2 h not only serves to functionalize the ends of the PF chains but also plays a role in controlling the polymerization degree (PD) in a statistical fashion. As a result, the M_n of the PF could be limited to be around 3000. Such molecular weight is reasonable as it offers enough solubility for PF in the reaction mixture at enhanced temperature, which is critical to initiate further ATRP. Esterification of the above polymer with 2-bromoisobutyryl bromide afforded the final macroinitiator. 2-Bromoisobutyrate derivatives have proven to be versatile for ATRP of many vinyl monomers [28]. The structures of both PFOH and the PF

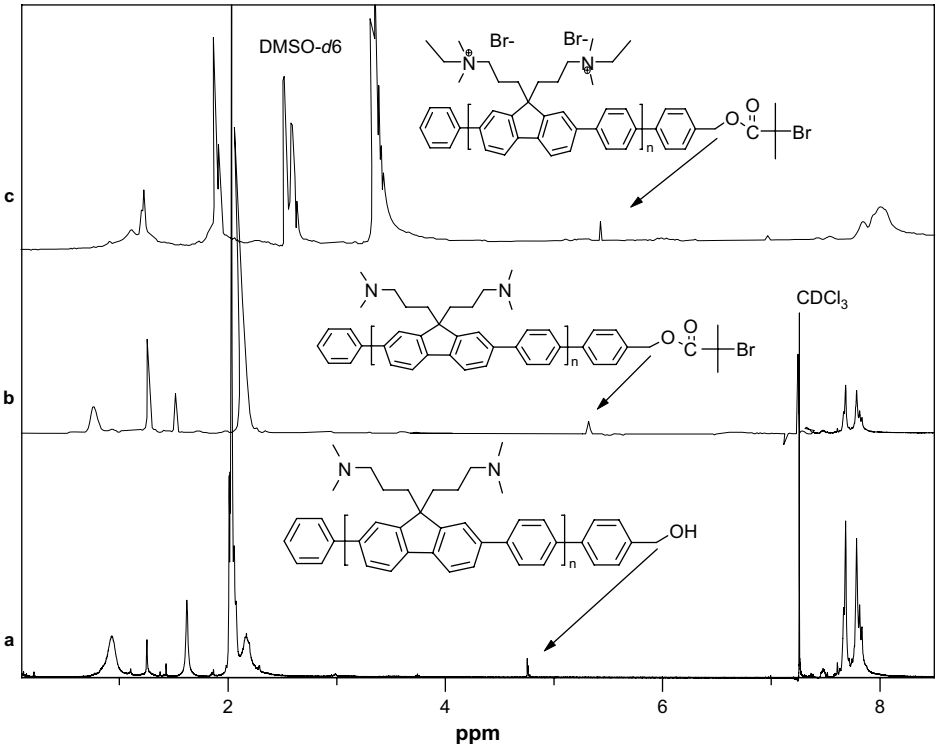

Fig. 1. ^{1}H NMR spectra of PF–OH, PF–Br and PF-M.

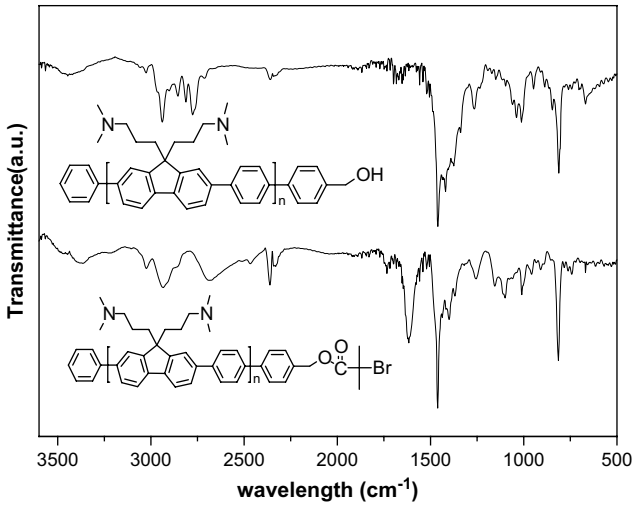

Fig. 2. FTIR spectra of PF–OH and PF–Br.

macroinitiator were confirmed by ^{1}H NMR, ^{13}C NMR, and FTIR spectroscopy. Fig. 1 shows the ^{1}H NMR spectra of PF–OH and the PF macroinitiator. The distinct peaks exhibited in both spectra between 7.50 and 7.65 ppm clearly show the successful incorporation of the end-capping phenylene groups. In addition, compared with Fig. 1a, Fig. 1b shows thorough suppression of the resonance for Ph–CH_2–OH at 4.81 ppm and appearance of a single resonance for Ph–CH_2–OC═O at 5.31 ppm, indicating a complete transformation of the hydroxyl into bromoisobutyrate functionality in the macroinitiator. The FTIR spectrum of the PF macroinitiator is compared with that of PFOH, as shown in Fig. 2. The appearance of the peak at 1737 cm^{-1} for the PF macroinitiator also proves the successful functionalization with 2-bromoisobutyrate in the end of the macroinitiator chain. The PD of the PF macroinitiator was estimated by comparing the relative integrations of total aromatic protons and the methylene protons (Ph–CH_2–OC═O). Thus, the number-average PD of the PF macroinitiator was calculated to be about 7, which is close to the result from GPC measurements.

Conversion of the neutral polymer macroinitiator to the corresponding cationic polymer macroinitiator was achieved by stirring with bromoethane in THF/DMSO (4:1) at 25 °C for 5 days. Post-quaternization approach has the advantage that the neutral polymers can be purified easily and characterized clearly [29]. The solubility of the quaternized polymers is different from their neutral precursors. The neutral polymer is readily soluble in common organic solvents such as THF, chloroform, toluene, and xylene, but insoluble in DMSO and water. After quaternization, the resulted polymer is insoluble in THF and chloroform but completely soluble in DMSO, methanol, and DMF. Both the neutral and the quaternized polymers have good solubility in the aqueous acetic acid or its mixture with other organic solvents such as methanol, due to weak interaction between the nitrogen atoms in amino and ammonium groups in the side chain and the acetic acid [29].

Fig. 1c shows the ^{1}H NMR spectra of the quaternized PF macroinitiator in DMSO-d_6. It can be seen that a new peak is exhibited at 3.35 ppm due to the successful quaternization of the amine residues in the PF blocks. For the neutral polymer macroinitiator, the signals corresponding to the methyleneamino and methylamino groups were mixed together with the peaks for the methylene (–CH_2–) groups adjacent to the 9-position carbon atoms of the fluorene rings, in the region around 2.20–1.95 ppm. After treatment with the bromoethane, all signals for the methylene (–CH_2N, –NCH_2CH_3) and methyl (–NCH_3) groups adjacent to the nitrogen atoms shift to the lower field region (3.35 ppm). The quaternization degrees of water-soluble polymer macroinitiator could be determined by the shift of ^{1}H NMR spectra. The relative intensities of these two peaks can be used to estimate the quaternization degrees. It is also noted that there is always some water remaining in the quaternized polymers [30], even after the copolymers were dried in vacuum at 150 °C for a long time. The amount of water in the polymers was estimated to be about 2% by thermogravimetric analysis (TGA) for water-soluble polymer macroinitiator.

ATRP of NIPAM was conducted at 60 °C in DMSO solution with CuCl/HMTETA as the catalytic system. A linear relationship was observed in the first-order kinetic plot (Fig. 3), indicating the presence of a constant number of the growing species during the polymerization. It is proposed that halogen exchange would occur between chlorine and terminal bromine when CuCl is used as catalyst in a bromine ended initiation system, which results in the formation of chlorine-ended polymer chains as the reaction proceeds [31]. Such a halogen exchange would make the initiation faster than the chain propagation and be beneficial to ATRP. The linear increase of the molecular weight and narrow molecular weight distribution (MWD) of the resulting copolymers supports the controlled fashion of the ATRP of NIPAM, as shown in Fig. 4.

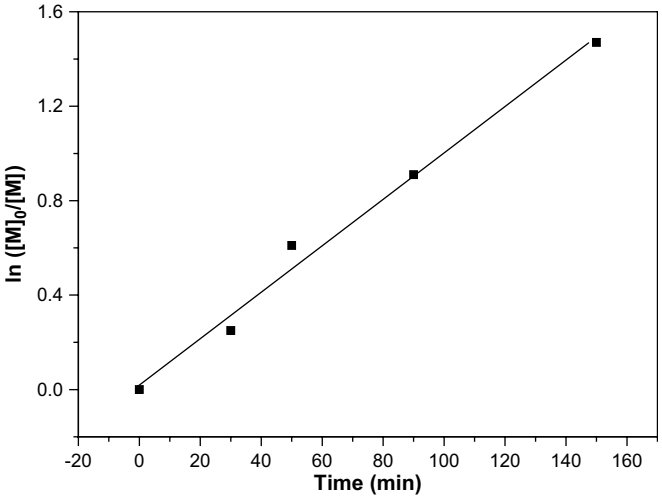

Fig. 3. ln([M]$_0$/[M]) vs polymerization time for ATRP of NIPAM with [polyfluorene]:[CuCl]:[HMTETA]:[NIPAM]$_0$ = 1:2:2:150, 50 vol% in DMSO, 60 °C (NIPAM = *N*-isopropylacrylamide; HMTETA = 1,1,4,7,10,10-hexamethyltriethylenetetramine).

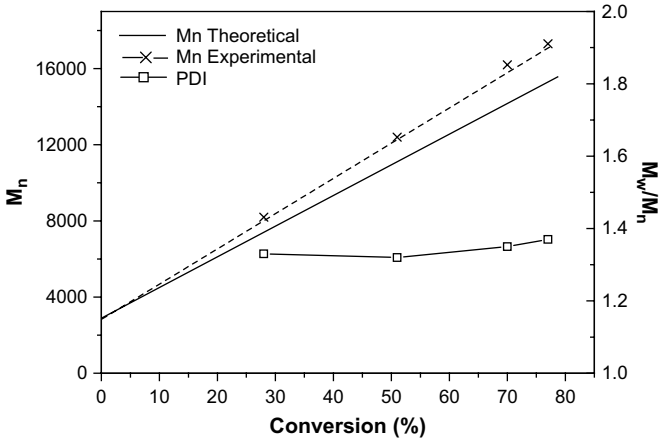

Fig. 4. Dependence of molecular weight (GPC) and molecular weight distribution (PDI) on monomer conversion for ATRP of NIPAM with [polyfluorene]:[CuCl]:[HMTETA]:[NIPAM]$_0$ = 1:2:2:150, 50 vol% in DMSO, 60 °C (NIPAM = *N*-isopropylacrylamide; HMTETA = 1,1,4,7,10,10-hexamethyltriethylenetetramine; PDI = polydispersity index).

Table 1
ATRP results of NIPAM initiated by PF macroinitiator (PF-M).[a]

Sample	[M]/[I][b]	Time (min)	Conv (%)	$M_{n,theo}$	$M_{n,NMR}$	$M_{n,GPC}$	M_w/M_n
PF-*b*-PNIPAM$_{23}$	25	90	82	5400	5900	5700	1.26
PF-*b*-PNIPAM$_{42}$	50	90	78	7500	8500	7800	1.25
PF-*b*-PNIPAM$_{88}$	100	100	79	12 000	11 500	13 100	1.43
PF-*b*-PNIPAM$_{45}$	150	30	28	7800	8000	8200	1.33
PF-*b*-PNIPAM$_{82}$	150	50	45	10 700	10 700	12 400	1.32
PF-*b*-PNIPAM$_{116}$	150	90	60	13 300	16 000	16 200	1.35
PF-*b*-PNIPAM$_{126}$	150	150	77	16 100	18 000	17 300	1.37

[a] [HMTETA]:[CuCl]:[I] = 2:2:1; ratio of monomer (NIPAM) vs solvent (DMSO) in volume was 1:1. All the reactions were conducted at 60 °C.
[b] [I] is defined as the molar concentration of PF macroinitiator containing 7 fluorene units and two benzene rings with initiating groups (NIPAM = *N*-isopropylacrylamide; PF = polyfluorene; HMTETA = 1,1,4,7,10,10-hexamethyltriethylenetetramine).

Because the macroinitiator was obtained through a step-growth polymerization approach where the molecular weight is controlled by the ratio of the end-capper instead of the polymerization mechanism, the PF macroinitiator presented a poorly controlled MWD (M_w/M_n was as high as 1.5). However, all the copolymers obtained by ATRP showed relatively narrow MWD (Table 1). The considerable decrease of MWD values of the block copolymers compared with that of the macroinitiator should be attributed to the well-defined PNIPAM chains existing in the copolymers. Table 1 summarizes the ATRP results of the copolymers.

The formation of block structures can be evidenced by GPC measurement. Fig. 5 shows the GPC profiles of the PF macroinitiator and four copolymer samples prepared using CuCl/HMTETA as the catalyst. The GPC curves corresponding to the respective block copolymers steadily shifted to high molecular weights with the increase of monomer conversion, implying a well-controlled polymerization. All the GPC traces gave symmetrical shapes without shoulder, indicating the efficient initiation of NIPAM by the PF macroinitiator. Moreover, in all the GPC profiles of the block copolymers, no peak was observed with the retention time for the macroinitiator, indicating that well-functionalized macroinitiator was prepared at the first stage and relatively complete incorporation of the macroinitiator into the final copolymers has been achieved. These results clearly prove the successful preparation of the diblock copolymers.

The structures of the block copolymers were confirmed by ^{1}H NMR (Fig. 6). The signals from the aromatic protons of the block copolymers are almost identical to those of the PF macroinitiator except for the slightly different chemical shifts of the end phenyl protons, due to the change in the neighboring chemical environment after polymerization. In Fig. 6, the proton absorption for Ph–C*H*$_2$–OC═O at 5.31 ppm arising from the PF macroinitiator thoroughly disappeared, and a new split peak was observed at 3.81–3.83 ppm, which is ascribed to the –NH–C*H*(CH$_3$)$_2$ protons. These results strongly suggest the formation of well-defined block copolymers through ATRP with efficient initiation of NIPAM and perfect intactness of PF backbone. The resulting block copolymers (PF-*b*-PNIPAM) were readily soluble in many common solvents including DMSO, DMF, methanol and water.

3.2. Stability analysis

The thermal stability of the quaternized polymers in nitrogen was evaluated by thermogravimetric analysis (TGA). The thermograms are depicted in Fig. 7. The quaternized polymers possess fair thermal stability. These salts started to decompose at ca. 200 °C, with a small amount of water loss at lower temperatures. This phenomenon was also observed in our previous work due to the excellent hydrophilic properties of the polymers synthesized [32]. The small amount of water (<3 wt%) cannot be removed completely by increasing temperature in vacuum, which usually results in experimental errors for element analysis. The modified method could be successful to analyze water-soluble polymers. For example, the water present in the elemental analysis results was based on mass loss in the TGA and the bromide determination was carried out by Schöniger combustion method and then by titration with $HgNO_3$ [33]. In Fig. 7, the onset degradation temperature of PF-M was located at 240 °C in nitrogen, whereas for PF-*b*-PNIPAM it was about 200 °C. The 5% weight loss temperatures for PF-*b*-PNIPAM$_{23}$, PF-*b*-PNIPAM$_{42}$, and PF-*b*-PNIPAM$_{116}$ samples are 230, 210 and 190 °C, respectively. The higher degradation temperature of PF-M is due to more phenyl and fluorene in PF-M main chains than in PF-*b*-PNIPAM. Consequently, PF-*b*-PNIPAM possesses the lower degradation temperature due to the presence of methyl and NIPAM in its main chains. From Fig. 7, it can be seen that the degradation for all the polymers takes place by multiple steps. The first mass loss comes from quaternized salts, as reported by Balanda et al. [33]. The second major transition occurred in the vicinity of the first transition, probably due to the side chain cleavage of C–C and main chain C–C bonds of NIPAM. The residual mass at 550 °C is approximately 40%, 38%, 25% and 10% of the starting mass for PF-M, PF-*b*-PNIPAM$_{23}$, PF-*b*-PNIPAM$_{42}$, and PF-*b*-PNIPAM$_{116}$, respectively. The combustion char mainly comprises carbon char. In air atmosphere, the decomposition temperature and residual mass were slightly lower, compared with those in nitrogen.

3.3. Optical properties

Fig. 8 shows UV–vis absorption and PL spectra of PF-M and PF-*b*-PNIPAM$_{116}$ in the solution of several solvents in a concentration of 1×10^{-6} M based on the polymer repeat unit. In Fig. 8, the absorption peaks of PF-M in methanol, DMF, and H_2O are observed at 385, 389, and 393 nm, respectively. The corresponding PL spectrum is peaked at 416, 417, and 421 nm with the vibronic shoulder around 434, 436, and 440 nm, respectively. Absorption peaks of PF-*b*-PNIPAM$_{116}$ in methanol, DMF, and water are 386, 389, and 394 nm, respectively. The corresponding PL spectrum is peaked at 421, 425, and 430 nm with the vibronic shoulder around 444, 450, and 454 nm, respectively. The remarkably increased red-shift in both absorption and PL spectra for PF-M and PF-*b*-PNIPAM$_{116}$ as increasing polarity of solvent can be explained by the increased torsion angle of the polymer main chains, due to the increased repulsion between the positive ammonium groups in the side chains and the adjacent fluorene units in the polar solvents. Another possible explanation for such red-shift is the increase in chain aggregation of the polymer main chains of the polyelectrolytes in the polar solvents. Tan et al. reported that PPE–SO^{3-} (sulphonated poly(phenylene ethynylene)) showed PL spectra with a maximum peak at 447 nm and distinct vibronic shoulders, which is typical for non-aggregated PPEs in good solvents [35]. In contrast, in the polar solvent, PPE–SO^{3-} shows a broad PL peak with

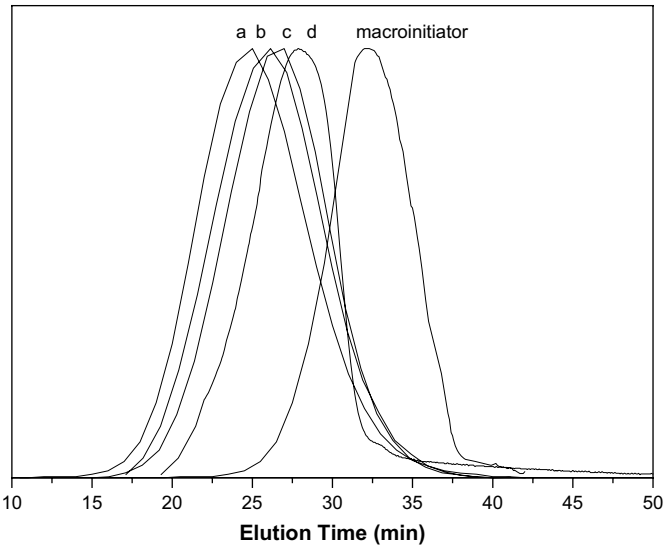

Fig. 5. GPC traces of polyfluorene macroinitiator (THF) and diblock copolymers PF-*b*-PNIPAM (water): (a) conversion = 28%, M_n (GPC) = 8200, M_w/M_n = 1.33; (b) conversion = 45%, M_n (GPC) = 12 400, M_w/M_n = 1.32; (c) conversion = 60%, M_n (GPC) = 16 200, M_w/M_n = 1.35; (d) conversion = 77%, M_n (GPC) = 17 300, M_w/M_n = 1.37. Reaction conditions: [polyfluorene]:[CuCl]:[HMTETA]:[NIPAM]$_0$ = 1:2:2:150, 50 vol% in DMSO, 60 °C (NIPAM = *N*-isopropylacrylamide); HMTETA = 1,1,4,7,10,10-hexamethyltriethylenetetramine.

a maximum moved to 550 nm, which is typical for excimer-like photoluminescence. The authors suggested that the tendency for aggregation of polymer electrolyte in a strong polar solvent is due to the increased face-to-face π-stacking between phenylenes in the adjacent chains [34]. Thus, the red-shift of absorption and PL emission spectra of polyelectrolytes in polar spectra should be related to the increase in the chain conjugation.

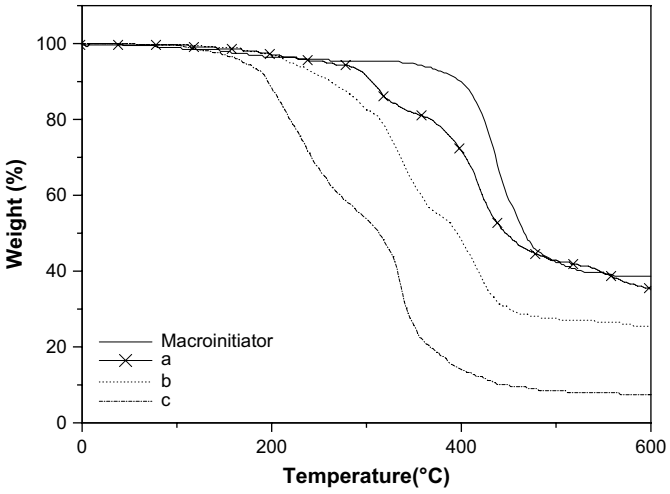

Fig. 7. Thermogravimetric traces of polyfluorene macroinitiator and diblock copolymers PF-*b*-PNIPAM: (a) PF-*b*-PNIPAM$_{23}$; (b) PF-*b*-PNIPAM$_{42}$; (c) PF-*b*-PNIPAM$_{116}$.

From the application point of view, one of the most attractive properties of the polymer synthesized is the relatively high PL quantum yield (Φ_{pl}). Both the neutral polymer and the quaternized polymers displayed blue fluorescence in solutions upon exposure to UV light. The Φ_{pl} values of the dilute aqueous solutions of PF-M and PF-*b*-PNIPAM$_{116}$ were measured to be as high as 28% and 32%, respectively, when using the quinine sulfate solution (ca. 1.0×10^{-5} M) in 0.10 M H_2SO_4 (quantum yield, 55%) as a standard [35]. When the measurement was conducted in aqueous solution with the increase of temperature from 15 °C to 40 °C, the corresponding values of Φ_{pl} were 28% and 25% for PF-M and PF-*b*-PNIPAM$_{116}$, respectively. The decreased PL efficiency of PF-*b*-PNIPAM$_{116}$ may be attributed to the aggregation of the polymer chains in

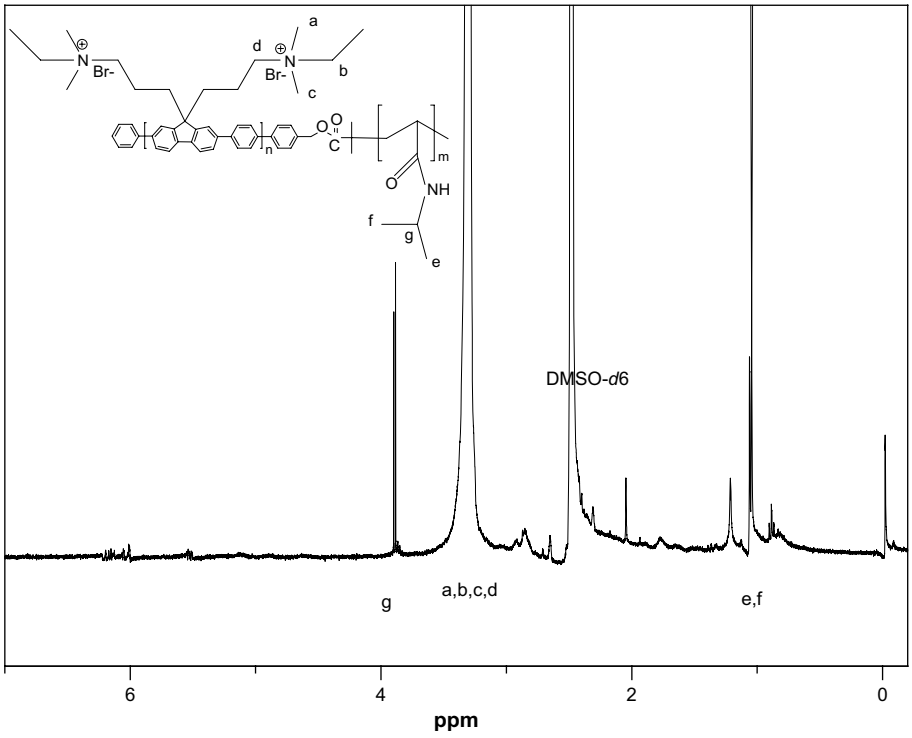

Fig. 6. ^{1}H NMR spectra of water-soluble PF-*b*-PNIPAM$_{116}$ diblock copolymer in DMSO-d_6.

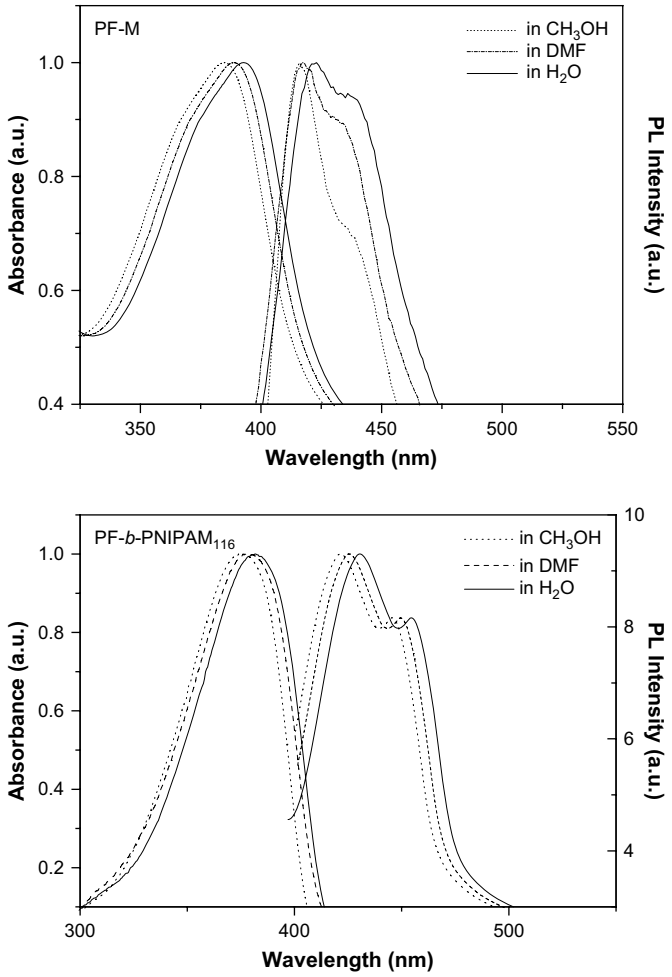

Fig. 8. UV–vis absorption and PL emission spectra of PF-M and PF-*b*-PNIPAM$_{116}$ diblock copolymers. The concentration of polymer in measurement is 1.0×10^{-6} M. PF-*b*-PNIPAM$_{116}$ diblock copolymers: conversion = 60%, M_n (GPC) = 16200, M_w/M_n = 1.35. Reaction conditions: [polyfluorene]:[CuCl]:[HMTETA]:[NIPAM]$_0$ = 1:2:2:150, 50 vol% in DMSO, 60 °C (NIPAM = *N*-isopropylacrylamide); HMTETA = 1,1,4,7,10,10-hexamethyltriethylenetetramine.

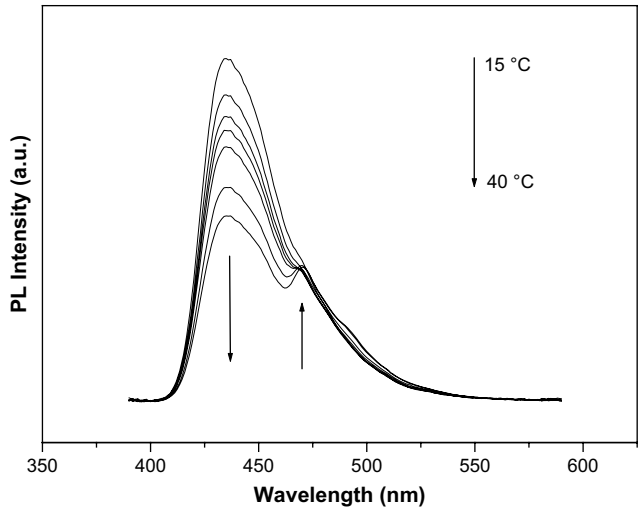

Fig. 9. Temperature dependence of PL emission spectra of PF-*b*-PNIPAM$_{116}$ diblock copolymers.

aqueous solution. This was supported by a further reduced PL efficiency measured in methanol solution as increasing temperature from 15 °C to 40 °C (Fig. 9). In other words, PF-*b*-PNIPAM was found to create more obvious red-shifted absorption and fluorescence spectra than PF-M, as shown in Fig. 8. Such an increase of red-shift as increasing the measurement temperature is attributed to the thermoresponsive micellization behavior of NIPAM block in PF-*b*-PNIPAM.

3.4. Thermoresponsive micellization

PNIPAM homopolymer can be dissolved in cold and dilute aqueous solution but becomes insoluble above 32 °C due to the well-known lower critical solution temperature (LCST) phase behavior. Several research groups reported the thermoresponsive micellization behavior of polymer-*b*-PNIPAM, forming PNIPAM–core micelles stabilized by polymer chains in the corona [36–41]. Based on the previous reports on the water solubility of PDMAEMA–PF–PDMAEMA [DMAEMA = 2-(dimethylamino)ethyl methacrylate] [17] and PMAA–PF–PMAA [16], the water solubility of polyfluorene chains could be blocked by the presence of different contents of NIPAM monomers. In this case, PF-*b*-PNIPAM$_{116}$ was synthesized and used for subsequent studies of thermoresponsive micellization. PF-*b*-PNIPAM$_{116}$ is directly soluble in water at 15 °C. Upon heating to 40 °C, a bluish tinge characteristic of micellar solutions appears (Scheme 1). The temperature-dependent transmittance of a 1.0×10^{-5} M aqueous solution of PF-*b*-PNIPAM$_{116}$ is shown in Fig. 10. The transmittance starts to decrease considerably at 27 °C, indicating that PF-*b*-PNIPAM block copolymer is water insoluble due to its thermal phase transition. Above 40 °C, the transmittance stabilizes out, suggesting the complete thermo-induced micellization. Based on the chemical principle, the formed micelle should possess a core consisting of PNIPAM and a PF corona (Scheme 1). Compared to the LCST (32 °C) of PNIPAM homopolymer with similar molecular weight, the critical micellization temperature (CMT) (27 °C) observed for PF-*b*-PNIPAM$_{116}$ block copolymer is slightly lower. This is quite reasonable because hydrophobic PF residues are incorporated into PNIPAM block. It is well known that the LCST behavior of PNIPAM homopolymer can be finely tuned when they are random or block copolymerized with hydrophilic or

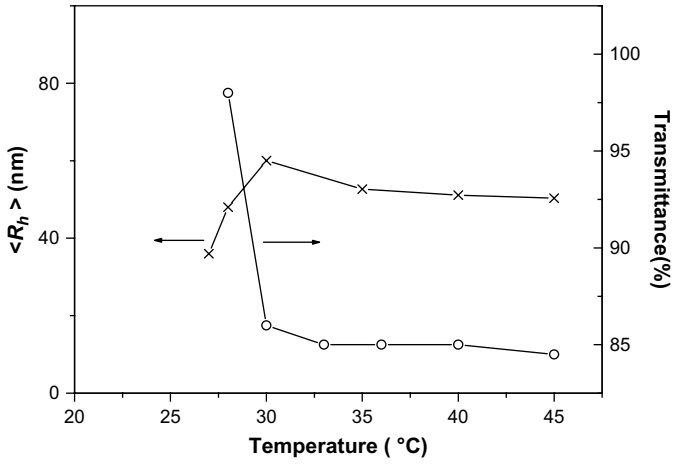

Fig. 10. Temperature dependence of the average hydrodynamic radius, $\langle R_h \rangle$, and optical transmittance for PF-*b*-PNIPAM$_{116}$ diblock copolymers. The concentration of polymer aqueous solution: 0.15 g/L for LLS measurement and 1.0 g/L for transmittance measurement. PF-*b*-PNIPAM$_{116}$ diblock copolymers: conversion = 60%, M_n (GPC) = 16 200, M_w/M_n = 1.35. Reaction conditions: [polyfluorene]:[CuCl]:[HMTETA]:[NIPAM]$_0$ = 1:2:2:150, 50 vol% in DMSO, 60 °C (NIPAM = *N*-isopropylacrylamide); HMTETA = 1,1,4,7,10,10-hexamethyltriethylenetetramine.

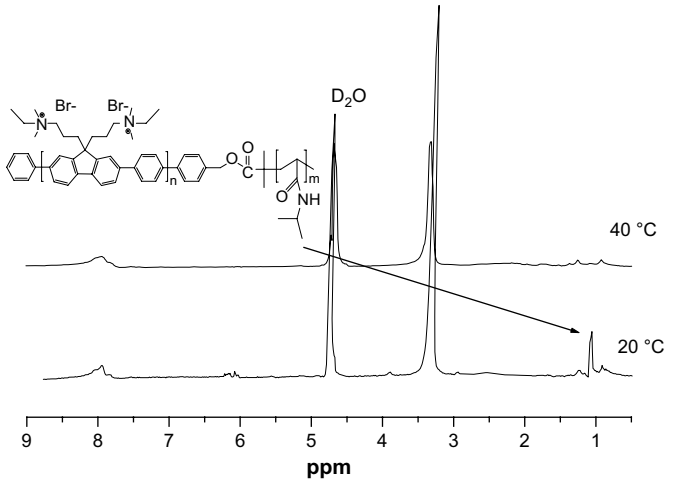

Fig. 11. ^{1}H NMR spectra of PF-*b*-PNIPAM$_{116}$ diblock copolymer in D_2O at different temperatures.

hydrophobic monomers, which can accordingly increase or decrease its LCST.

Dynamic LLS was employed to characterize the thermoresponsive micellization behavior. Fig. 10 shows typical hydrodynamic radius distributions, $f(R_h)$, of the aqueous solution of PF-*b*-PNIPAM$_{116}$ at different temperatures. At 20 °C, the diblock copolymer is molecularly dissolved and the average hydrodynamic radius, $\langle R_h \rangle$, cannot be detected. When increasing temperature from 25 °C to 32 °C, the solubility of PNIPAM block changes obviously, that is, the micellization of the diblock copolymer occurs. When the temperature is raised to 40 °C, the intensity-average hydrodynamic radius $\langle R_h \rangle$ is increased to 51 nm with a polydispersity of 0.11. The significant change of $\langle R_h \rangle$ and the dramatic increase of scattered light intensity at elevated temperatures probably indicate the formation of core–shell nanoparticles (Scheme 1).

The thermoresponsive micellization of PF-*b*-PNIPAM$_{116}$ was further investigated by ^{1}H NMR spectra in D_2O (Fig. 11). At 20 °C, the copolymer is fully solvated, and the characteristic signals of both blocks are visible. The signals at $\delta = 1.1$ ppm are the characteristic of NIPAM (see peak assignments in Fig. 11). At 40 °C, the ^{1}H NMR spectrum clearly shows the relative intensity of the characteristic signal of NIPAM. This indicates that the PNIPAM block becomes insoluble at 40 °C, leading to the formation of PNIPAM–core micelles stabilized by the well-solvated PF coronas.

3.5. Fluorescent quenching of polymers

One promising application of WSCPs is for chemosensors or biosensors due to their fluorescent superquenching by traces of analytes. The quenching of fluorescence generally includes static quenching and dynamic quenching. Each quenching behavior can be simply described by the Stern–Volmer equation [42]:

$$F_o/F = 1 + K_{sv}[Q] \quad (3)$$

where F_o is the fluorescence intensity without quencher; F is the fluorescence intensity with quencher present; [Q] is the quencher concentration, and K_{sv} is the Stern–Volmer constant. Both dynamic quenching and static quenching follow a linear Stern–Volmer plot (F_o/F–[Q]). However, if the dynamic quenching and static quenching exist simultaneously, Eq. (3) must be modified, and the plot usually shows an upward curve [42]:

$$F_o/F = \left(1 + K_{sv}^{S}[Q]\right)\left(1 + K_{sv}^{D}[Q]\right) \quad (4)$$

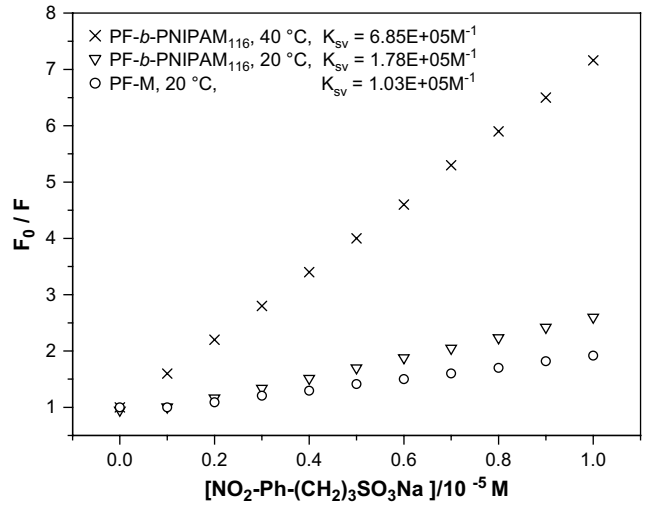

Fig. 12. The Stern–Volmer plot of PF-M, PF-*b*-PNIPAM$_{116}$ (20 °C) and PF-*b*-PNIPAM$_{116}$ (40 °C) [1.0×10^{-5} M] quenched by sodium 3-(4-nitrophenyl)propane-1-sulfonate.

where K_{sv}^{S} is the static quenching constant and K_{sv}^{D} is the dynamic quenching constant. Both linear and upward Stern–Volmer curves were observed previously with WSCPs [43,44]. The linear parts are consistent with the concept of "sphere-of-action", which means that the static quenching process is dominant. The non-linear parts were originated from the coexistence of static and dynamic quenching processes for aggregation of analyte with chromophore. In order to obtain the linear quenching curve, the experimental elements must be controlled.

Even though the oxygen plays a role in the PL quenching of polymer, the quenching phenomenon is equally observed in samples with and without oxygen. And, some other factors such as polymer concentration seem to be more important when dealing with quantitative results, indicating that the value of K_{sv} is not affected by the presence of oxygen but by the polymer concentration. Therefore, the linear Stern–Volmer plots were obtained by decreasing the concentration of polymer and quencher system, as shown in Figs. 12 and 13.

The quenching of PF-M, PF-*b*-PNIPAM$_{116}$ (20 °C) and PF-*b*-PNIPAM$_{116}$ (40 °C) by sodium 3-(4-nitrophenyl)propane-1-sulfonate is shown in Fig. 12. The K_{sv} values of PF-M, PF-*b*-PNIPAM$_{116}$ (20 °C),

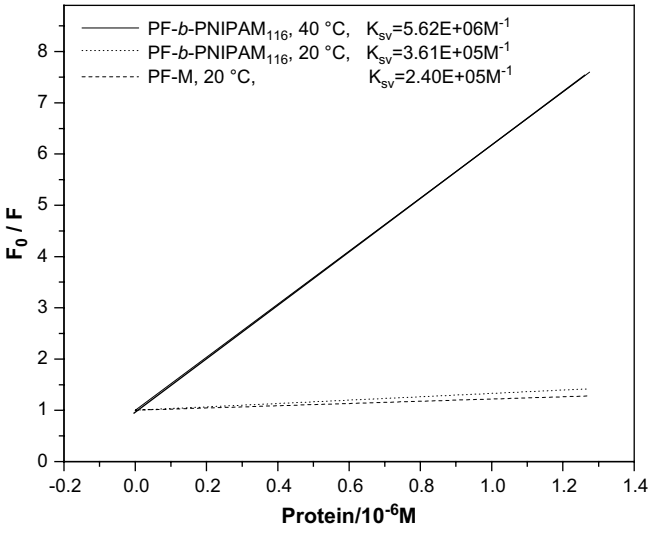

Fig. 13. The Stern–Volmer plot of PF-M, PF-*b*-PNIPAM$_{116}$ (20 °C) and PF-*b*-PNIPAM$_{116}$ (40 °C) [1.0×10^{-5} M] quenched by pepsase.

and PF-*b*-PNIPAM$_{116}$ (40 °C) are 1.03×10^5 M^{-1}, 1.78×10^5 M^{-1}, and 6.85×10^5 M^{-1}, respectively. The quenching sequence is PF-*b*-PNIPAM$_{116}$ (40 °C) > PF-*b*-PNIPAM$_{116}$ (20 °C) > PF-M. It means that PF-*b*-PNIPAM$_{116}$ at 40 °C has better selectivity than PF-*b*-PNIPAM$_{116}$ at 20 °C and PF-M for the thermoresponsive micellization behavior of PNIPAM. In order to prove that the thermoresponsive micellization behavior of PNIPAM has great effect on the quenching process, the quenching results of PF-M, PF-*b*-PNIPAM$_{116}$ (20 °C) and PF-*b*-PNIPAM$_{116}$ (40 °C) by pepsase are also shown in Fig. 13. The K_{sv} values of PF-M, PF-*b*-PNIPAM$_{116}$ (20 °C) and PF-*b*-PNIPAM$_{116}$ (40 °C) are 2.40×10^5 M^{-1}, 3.61×10^5 M^{-1} and 5.62×10^6 M^{-1}, respectively. Clearly, PF-*b*-PNIPAM$_{116}$ (40 °C) with thermoresponsive micellization behavior of PNIPAM has much more compact structure effect than those of PF-*b*-PNIPAM$_{116}$ (20 °C) and PF-M. Such a structure can be conjuncted to a range of secondary structures presented by protein macromolecules and has more conformational position to improve registry with analyte shape. At the same time, with better spatial interactions one can expect improved contacts between optically active groups and thus more efficient Förster resonance energy transfer.

4. Conclusions

In summary, we successfully synthesized a series of well-defined novel water-soluble diblock copolymers containing conjugated amino-terminal polyfluorene (PF) block and coil-like poly(*N*-isopropylacrylamide) (PNIPAM) through atom transfer radical polymerization initiated by a 2-bromoisobutyrate end-capped PF macroinitiator using CuCl/HMTETA (1,1,4,7,10,10-hexamethyltriethylenetetramine) as the catalyst. The chemical structures of block copolymers were characterized by ^{1}H NMR, UV–vis, and photoluminescence. The conjugated-ionic diblock copolymers obtained form PF aggregates in water, which is driven by the thermoresponsive micellization behavior of PNIPAM. And with the increase of temperature the diblock copolymers form PNIPAM–core micelles stabilized by PF chains in the corona, as confirmed by dynamic light scattering. The formation of excimers within the PF aggregates results in improved Förster resonance energy-transfer efficiencies.

Acknowledgements

This work was financially supported by the National Natural Science Foundation of China (20704009, 50403012), Shanghai Leading Academic Discipline Project (Project Number: B113), the Opening Project of Key Lab for Special Functional Materials, Henan University (0701).

References

[1] McQuade DT, Pullen AE, Swager TM. Chem Rev 2000;100:2537–74.
[2] Swager TM. Acc Chem Res 1998;31:201–7.
[3] Bunz UHF. Chem Rev 2000;100:1605–44.
[4] Yang JS, Swager TM. J Am Chem Soc 1998;120:11864–73.
[5] Gaylord BS, Heeger AJ, Bazan GC. J Am Chem Soc 2003;125:896–900.
[6] Jones RM, Bergstedt TS, McBranch DW, Whitten DG. J Am Chem Soc 2001;123:6726–7.
[7] Ho HA, Leclerc M. J Am Chem Soc 2003;125:4412–3.
[8] DiCesare N, Pinto MR, Schanze KS, Lakowicz JR. Langmuir 2002;18:7785–7.
[9] Liu B, Bazan GC. Nat Protoc 2006;1:1698–702.
[10] Thomas SW, Joly GD, Swager TM. Chem Rev 2007;107:1339–86.
[11] Pinto MR, Schanze KS. Synth Stuttg 2002;9:1293–390.
[12] Liu B, Bazan GC. Chem Mater 2004;16:4467–76.
[13] Wang S, Gaylord BS, Bazan GC. Adv Mater 2004;16:2127–32.
[14] Wang S, Bazan GC. Adv Mater 2003;15:1425–8.
[15] Gaylord BS, Heeger AJ, Bazan GC. Proc Natl Acad Sci U S A 2002;99:10954–7.
[16] Lu S, Fan QL, Liu SY, Chua SJ, Huang W. Macromolecules 2002;35:9875–81.
[17] Lu S, Fan QL, Liu SY, Huang W. Macromolecules 2003;36:304–10.
[18] Lu S, Liu TX, Ke L, Ma DG, Chua S, Huang W. Macromolecules 2005;38:8494–502.
[19] Liu S, Billingham NC, Armes SP. Angew Chem Int Ed 2001;40:2328–31.
[20] Schilli CM, Zhang M, Rizzardo E, Thang SH, Chong YK, Edwards K. Macromolecules 2004;37:7861–6.
[21] Xia Y, Burke NAD, Stolver HDH. Macromolecules 2006;39:2275–83.
[22] Zhang Y, Luo S, Liu S. Macromolecules 2005;38:9813–20.
[23] Zhang W, Zhou X, Li H, Fang Y, Zhang G. Macromolecules 2005;38:909–14.
[24] Wintgens V, Charles M, Allouache F, Amiel C. Macromol Chem Phys 2005;206:1853–61.
[25] Hofkens J, Hotta J, Sasaki K, Masuhara H, Taniguchi T, Miyashita T. J Am Chem Soc 1997;119:2741–2.
[26] Zhu X, DeGraaf J, Winnik FM, Leckband D. Langmuir 2004;20:10648–56.
[27] Huang F, Wu H, Wang D, Yang W, Cao Y. Chem Mater 2004;16:708–16.
[28] Matyjaszewski K, Xia J. Chem Rev 2001;101:2921–90.
[29] Liu B, Yu WL, Lai YH, Huang W. Macromolecules 2002;35:4975–82.
[30] Zhang X, Matyjaszewski K. Macromolecules 1999;32:1763–6.
[31] Wang WZ, Fan QL, Cheng F, Zhao P, Huang W. J Polym Sci Part A Polym Chem 2006;44:3513–25.
[32] Fan QL, Zhou Y, Lu XM, Hou XY, Huang W. Macromolecules 2005;38:2927–36.
[33] Balanda PB, Ramey MB, Reynolds JR. Macromolecules 1999;32:3970–8.
[34] Tan C, Pinto MR, Schanze KS. Chem Commun 2002;5:446–7.
[35] Harrison BS, Ramey MB, Reynolds JR, Schanze KS. J Am Chem Soc 2000;122:8561–2.
[36] Convertine AJ, Lokitz BS, Vasileva Y. Macromolecules 2006;39:1724–30.
[37] Yusa S, Shimada Y, Mitsukami Y. Macromolecules 2004;37:7507–13.
[38] Kizhakkedathu JN, Norris-Jones R, Brooks DE. Macromolecules 2004;37:734–43.
[39] Ray B, Isobe Y, Matsumoto K. Macromolecules 2004;37:1702–10.
[40] Zhang JX, Qiu LY, Zhu KJ. Macromol Rapid Commun 2004;25:1563–7.
[41] Jiang XZ, Ge ZS, Xu J. Biomacromolecules 2007;8:3184–92.
[42] Lakowicz JR. Principles of fluorescence spectroscopy. 2nd ed. New York: Plenum Press; 1999. p. 88–95.
[43] Chen L, McBranch DW, Wang HL, Helgeson R, Wudl F, Whitten DG. Proc Natl Acad Sci U S A 1999;96:12287–92.
[44] Wang J, Wang DL, Miller EK, Moses D, Bazan GC, Heeger AJ. Macromolecules 2000;33:5153–8.